Melt Rheological Behavior of PP–SAN Blend

S. N. MAITI,* VANITA AGARWAL, and A. K. GUPTA

Centre for Materials Science and Technology, Indian Institute of Technology, Delhi, New Delhi-110016, India

SYNOPSIS

A study of melt rheology of the blend of styrene–acrylonitrile (SAN) and polypropylene (PP) in composition range 0–50 wt % SAN content is presented. Measurements are made on a capillary rheometer at temperatures of 210, 230, and 250°C. The data are presented as flow curves and variations of melt viscosity and melt elasticity as functions of shear rate and blend composition. Scanning electron micrographs are presented to illustrate the dispersion and other characteristics of the SAN droplets. Results of melt rheology are interpreted in terms of the role of SAN droplets in the blend.

INTRODUCTION

Among the polyolefins isotactic polypropylene (PP) is one of the most useful and versatile polymers suitable for a wide range of applications. Its scope of applications has been widened further by blending it with a number of other polymers such as elastomers,[1-8] polyethylene,[9,10] poly(ethylene terephthalate),[11] polycarbonate,[12] polystyrene,[12,13] ABS copolymer,[14,15] etc. Improvements observed in the melt rheological properties of PP–SEBS,[1-6] PP–polybutadiene,[16] and PP–ABS[14,15] blend inspire us to undertake the present study of the blend of PP with styrene–acrylonitrile (SAN) copolymer. SAN copolymer has quite a useful combination of properties[17] that might show synergistic combinations with those of PP. The resulting blend is expected to be an immiscible one with accompanied disadvantages such as lower strength and modulus and advantages of improved processability and other properties. The role of dispersed-phase domains[1,2,14,18] in PP-based blends, recognized in the improvement of its melt processing behavior, is of interest to investigation in PP–SAN blend.

In the present work we present a study of the melt rheological properties of PP–SAN blend, prepared by melt blending technique. Melt rheological data such as shear stress, shear rate, melt viscosity, and melt elasticity parameters at blend compositions of 5–50 wt % SAN were generated on a piston-type capillary rheometer. Scanning electron microscopic measurements on cryogenically fractured surfaces of the extrudates are reported to illustrate the state of dispersion of SAN phase in the blend.

EXPERIMENTAL

Materials

PP used was Koylene M3030 (MFI 3, density 0.9 g/cm^{-1}) supplied by Indian Petrochemicals Corporation Ltd. The SAN copolymer used contained 28% AN with an intrinsic viscosity 1.38 dL/g and was obtained from Etino Quimica, South America.

Preparation of Blends

Blends of PP with SAN, with blend composition of 5–50 wt % SAN (on the basis of 100 parts PP) were prepared by melt mixing in a single screw extruder (Model BETOL BM 1820) at temperatures of 200–220°C at the feed zone and die zone, respectively. Thick strands coming out of the die were cooled under water and were granulated. These granules were fed to the capillary rheometer to generate rheological data.

Measurements

Melt flow properties were measured on a piston-type capillary rheometer (Koka Flow Tester of Shimadzu

Seisakusho, Ltd.) using circular die ($L/R = 40$) flat at the entrance region. Measurements were made in the pressure range of 10–110 kg/cm^2 at the three temperatures of 210, 230, and 250°C.

Scanning electron micrographs of the cryogenically fractured ends of the extrudates were recorded on a stereoscan (Model S4-10) of Cambridge Scientific Instruments Ltd. Micrographs were taken at magnification 500X.

RESULTS AND DISCUSSION

Melt Rheological Behavior

From the pressure difference, ΔP, at the entrance and exit of the capillary and the volumetric flow rate, Q, the apparent shear stress at wall, $(\tau_w)_{app}$, and apparent shear rate $\dot{\gamma}_{app}$ were calculated from the following expressions:[19]

$$(\tau_w)_{app} = \frac{\Delta P}{2(L/R)} \qquad (1)$$

$$(\dot{\gamma})_{app} = \frac{4Q}{\pi R^3} \qquad (2)$$

where L is the length and R is the radius of the capillary used.

These data were used to determine the value of the exponent n of the following power law:[19]

$$(\tau_w)_{app} = K(\dot{\gamma}_{app})^n \qquad (3)$$

The n thus determined was used to apply the Rabinowitsch correction to obtain true shear rate $\dot{\gamma}$, through the expression[19]

$$\dot{\gamma} = \frac{3n + 1}{4n} (\dot{\gamma}_{app}) \qquad (4)$$

Bagley correction on shear stress was considered negligible for the present case of high L/R of the capillary used. Hence $(\tau_w)_{app}$ may be taken as the true shear stress at wall τ_w.

The power law exponent[19] n' [corresponding to Eq. (5)] determined from the slopes of the flow curves (Figs. 1–3) has values shown in Table I.

$$\tau_w = K'\dot{\gamma}^{n'} \qquad (5)$$

Values of n' are between 0.4 and 0.6 for the PP–SAN blend in the entire range of blend composition
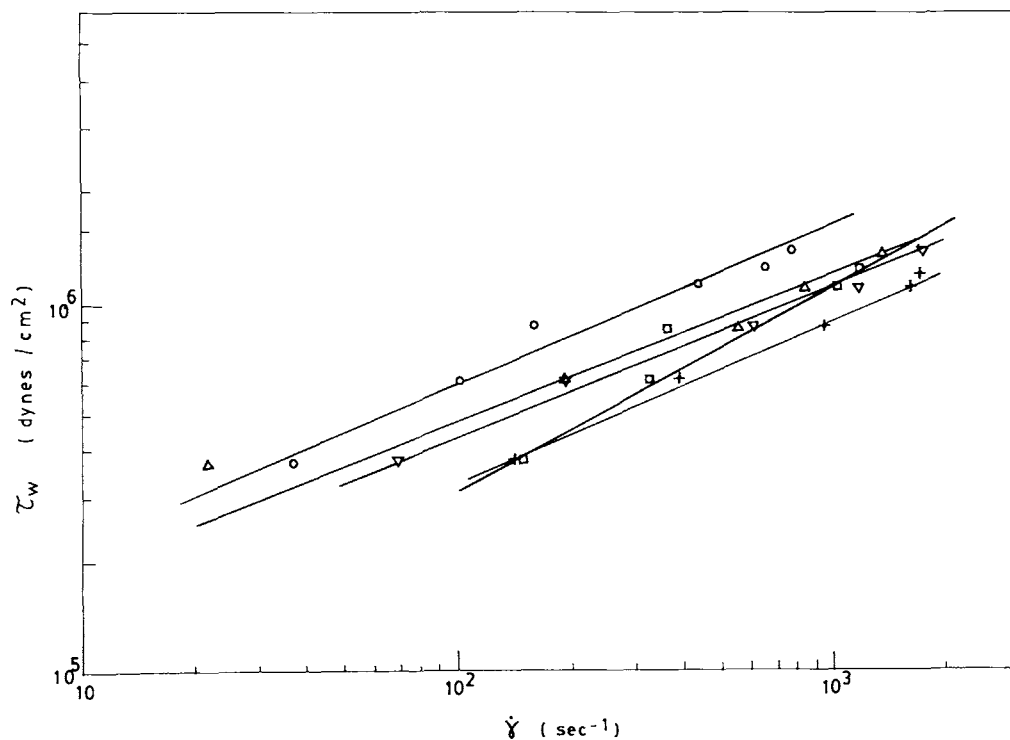
Figure 1 Flow curves of PP–SAN blend at 210°C at various compositions (wt % SAN):
(○) 0; (△) 10; (▽) 20; (□) 30; (+) 50.
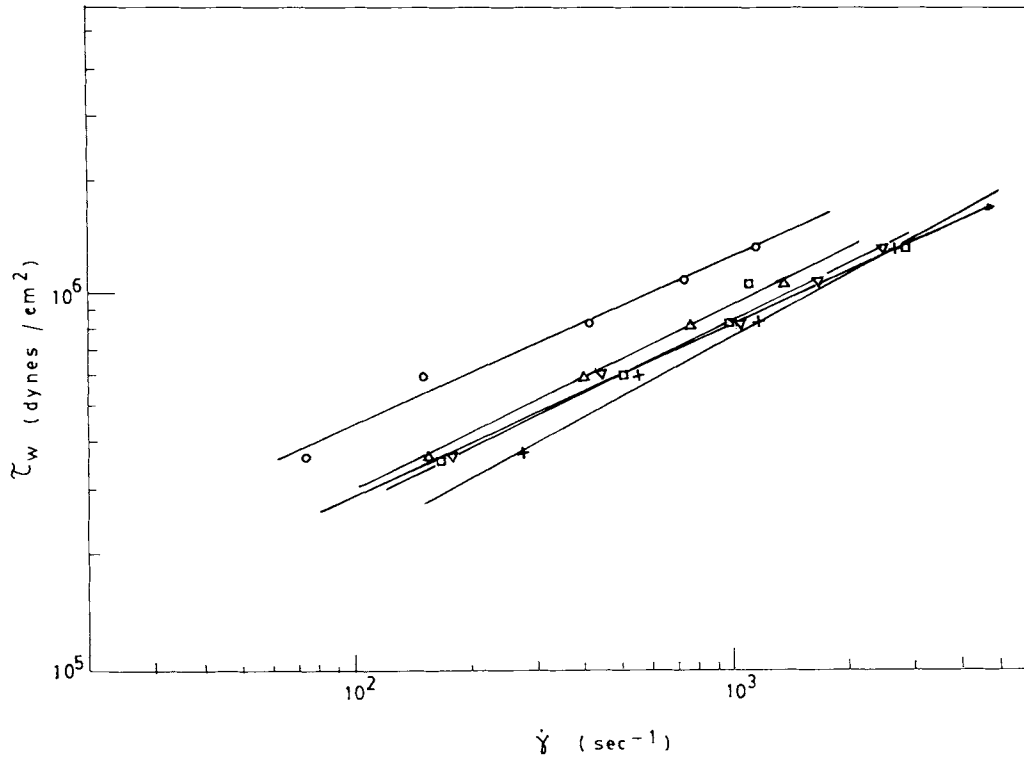
Figure 2 Flow curves of PP-SAN blend at 230°C at various compositions (wt % SAN):
(○) 0; (△) 10; (▽) 20; (□) 30; (+) 50.
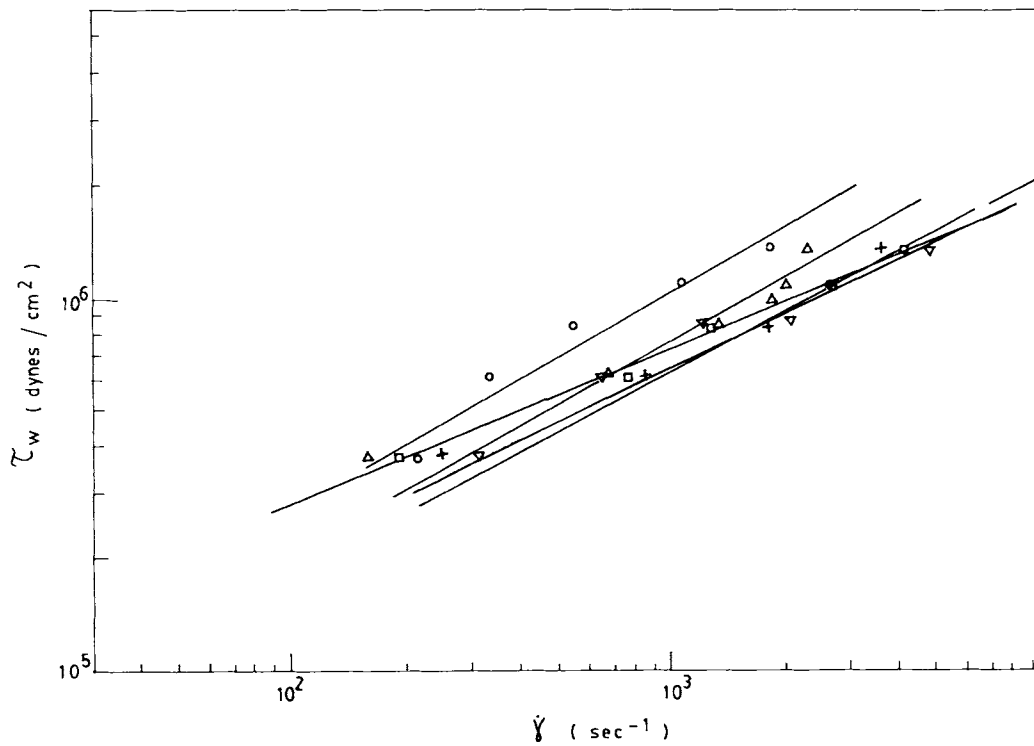
Figure 3 Flow curves of PP-SAN blend at 250°C at various compositions (wt % SAN):
(○) 0; (△) 10; (▽) 20; (□) 30; (+) 50.

Table I Values of Power Law Exponent n' [eq. (3)] for PP-SAN Blend

Blend Composition (wt % SAN)	n'		
	210°C	230°C	250°C
0	0.42	0.46	0.59
10	0.40	0.49	0.57
20	0.41	0.49	0.54
30	0.39	0.40	0.42
50	0.44	0.50	0.51

and temperature studied. At any given blend composition n' increases with increasing temperature. Whereas at any fixed temperature, the variation of n' with blend composition is small and irregular. At 250°C, n' exceeds 0.5, i.e., the limiting value for pseudoplastic behavior. This change in pseudoplasticity of the melt has two features: (1) the effect of temperature is almost identical for the blend as well as unblended PP and (2) the effect of blending ratio at any fixed temperature is significant, which indicates the role of the SAN component. The second effect becomes prominent with increasing temperature, which might be the effect of variation of the viscosity ratio of the two components with temperature.

Melt viscosity of the PP-SAN blend, which is of the order of 10^3–10^4 P in the studied range, decreases with shear rate linearly on log-log scale (Fig. 4). Variation of melt viscosity with blend composition is shown in Figure 5. Melt viscosity decreases with increasing SAN content quite rapidly up to 20 wt % SAN and then the decrease becomes slower. The total decrease in the studied blend composition range, which is a measure of the sharpness of the variation, decreases with increasing shear stress. Such an effect of shear stress on melt viscosity of a two-phase blend is due to the deformation of the dispersed-phase droplets during the flow. In the force field of applied shear stress, the dispersed droplets get elongated and aligned in the direction of flow, thus causing ease of flow or reduction in viscosity.

As we shall see in a latter section, the droplet size increases with increasing SAN content in this blend. Since larger droplets are easier to deform, one would expect greater ease of flow (or smaller viscosity) at higher SAN content, as is actually observed. Furthermore, the droplet deformability is more sensitive to the external applied force (i.e., shear stress) than to the size of the droplet, hence the variation of melt
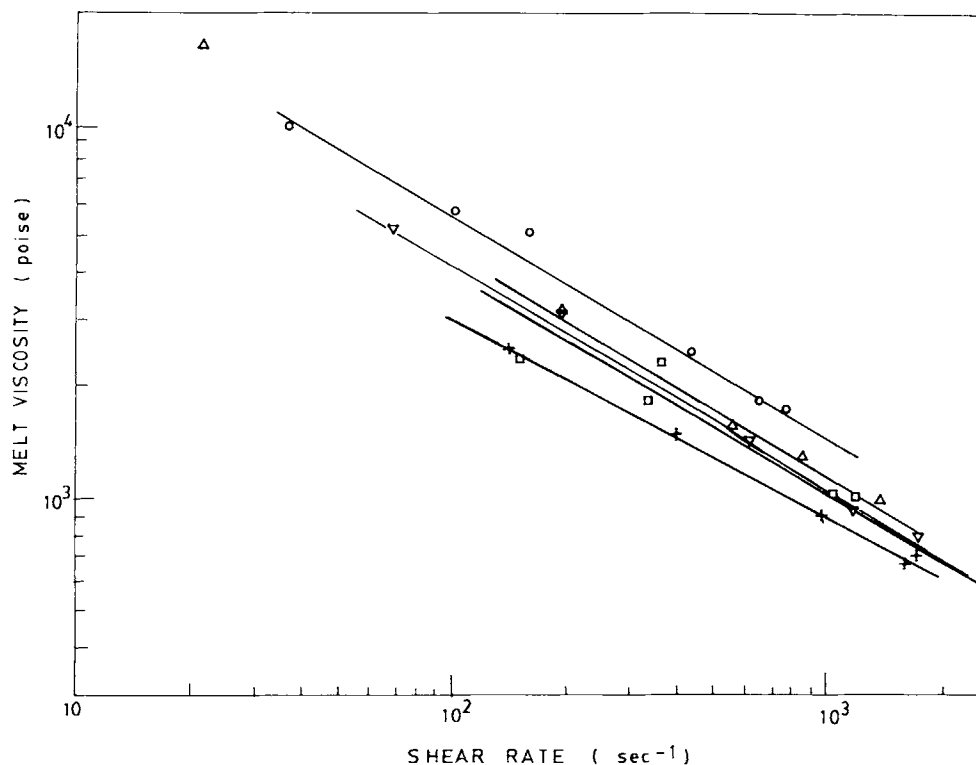
Figure 4 Variation of melt viscosity with shear rate for PP-SAN blend at 210°C at various compositions (wt % SAN): (O) 0; (△) 10; (▽) 20; (□) 30; (+) 50.
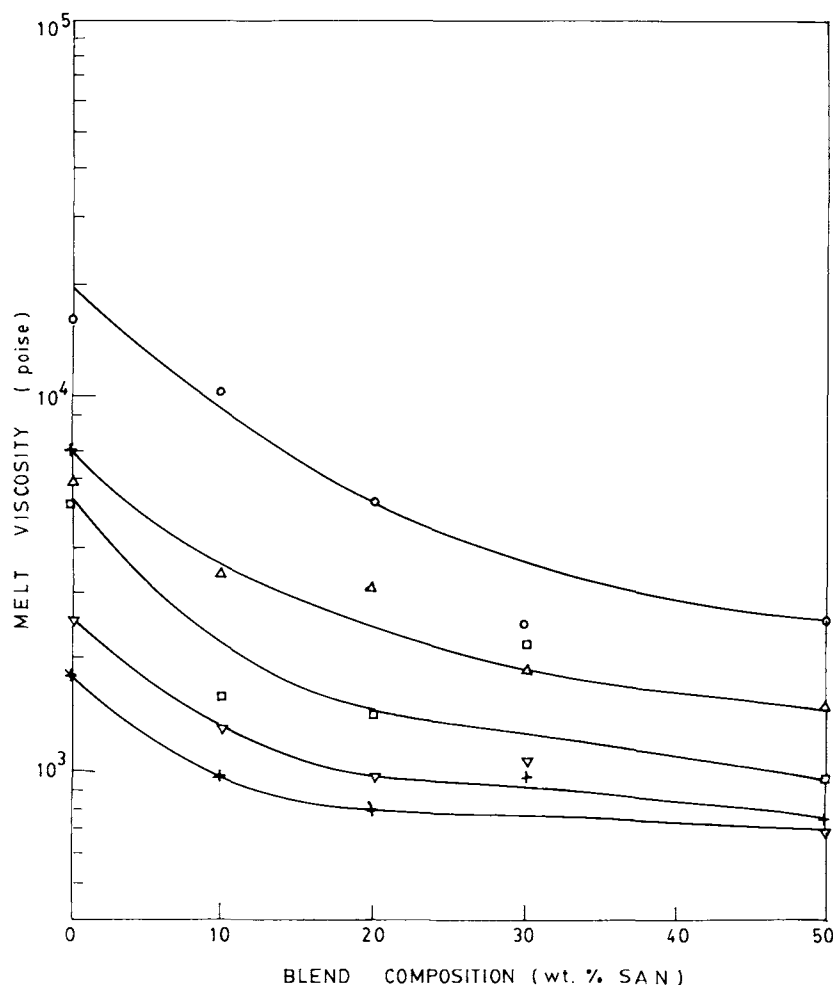
Figure 5   Variation of melt viscosity with blend composition at 210°C for PP–SAN blend at various shear stresses ($\times$ 10^5 dyn/cm^2): (O) 3.67; ($\triangle$) 6.12; ($\square$) 8.57; (∇) 11.2; (+) 13.5.

viscosity with blend composition becomes smaller at higher shear stress, as seen in Figure 5.

Arrhenius plots from these data at a shear stress 6.12×10^5 dyn/cm^2 are shown in Figure 6. Despite some scatter of data points, linear extrapolations are possible at all the compositions of the blend. The other possibility could be to draw a curve of continuously changing slope for each composition of the blend. This latter extrapolation is not done owing to the limited number of data points. However, as indicated from the varying slope of the Arrhenius plot the activation energy increases with increasing temperature. Thus the activation energies calculated from the linear extrapolations represent average values over the studied temperature range. These average values of activation energy, shown in Table II, decrease continuously with increasing SAN content of the blend. The decrease of activation en-

ergy is accompanied by the decrease of melt viscosity of the blend with increasing SAN content. Thus, SAN droplets, by virtue of their easy deformability, ease the flow and reduce the activation energy for viscous flow.

Melt elasticity, which governs the extrudate swell ratio of the melt, is commonly represented by the following parameters: first normal stress difference (τ_{11}–τ_{22}) and/or recoverable shear strain S_R. The recoverable shear strain, which is also a dimensionless quantity, is preferably used[20-22] to represent melt elasticity of two-phase blends. S_R is calculated from the measured extrudate swell ratio, through the expression[23]

$$S_R = [2(D_j/D)^6 - 2]^{1/2} \qquad (6)$$

where D_j and D are the diameters of the extrudate
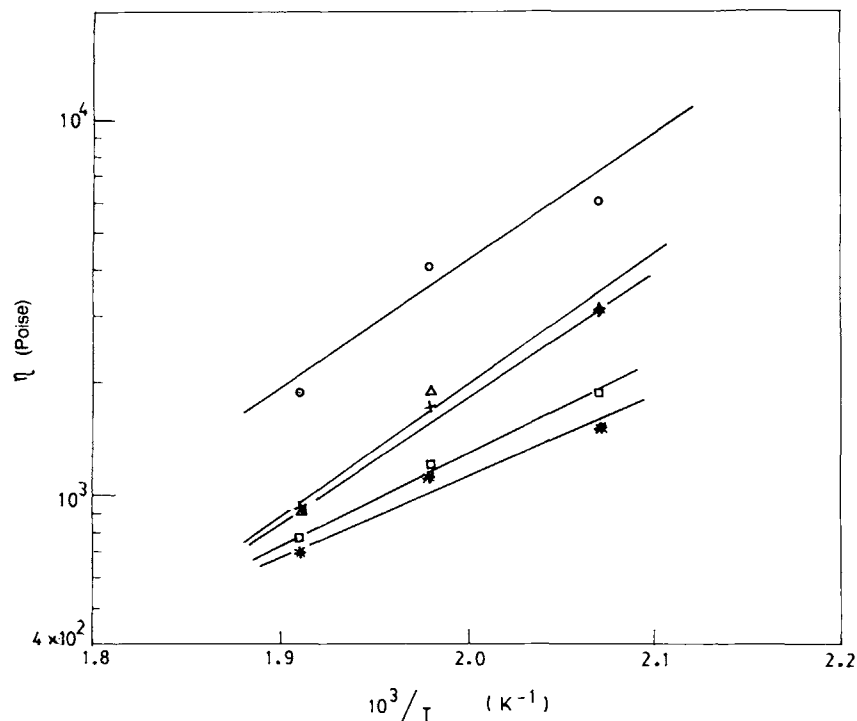
Figure 6 Arrhenius plots, log (melt viscosity) versus reciprocal temperature, for PP–SAN blend at shear stress 6.12×10^5 dyn/cm^2 for various blend compositions (wt % SAN): (○) 0; (△) 10; (+) 20; (□) 30; (∗) 50.

and the die, respectively, D_j/D is the extrudate swell ratio.

Variations of S_R with shear rate for PP–SAN blend, at the three temperatures of measurements, are shown in Figures 7–9. Melt elasticity (i.e., S_R) is in general lower for the blend than for the unblended PP and decreases with increasing SAN content of the blend. Difference of melt elasticity of the blend at various SAN contents reduces with increasing temperature, as seen from the decreasing separation of S_R versus $\dot{\gamma}$ curves at the three temperatures (Figs. 7–9).

The increase of S_R with shear rate is sufficiently linear for unblended PP but not so for the blend,

Table II Activation Energy ΔE for Viscous Flow for PP–SAN Blend

Blend Composition (wt % SAN)	ΔE (kcal/mol)
0	2.96
10	3.04
20	2.91
30	2.13
50	1.87

where two linear portions are distinguishable above and below the shear rate 10^3 s^{-1}. Increase of melt elasticity is faster at higher shear rates ($\gamma > 10^3$ s^{-1}) than at the lower shear rates. This effect is prominent at all the temperatures of measurements, only in the blend and not in the unblended PP, thus emphasizing the role of the second component of the blend (i.e., SAN).

As we shall see in a latter section, this blend forms a two-phase morphology with SAN droplets dispersed in the PP matrix. The recoverable shear strain for such a blend would be dependent on the elastic recoverability of the dispersed SAN droplets. Scanning electron micrographs present direct evidence for an increase of droplet size with increasing SAN content. This observation, when viewed in conjunction with the decrease of melt elasticity of the blend with increasing SAN content suggests that larger droplets are less elastic (or have lower recoverability) than the smaller droplets. Larger droplets have greater degrees of freedom, hence in the process of elastic recovery they may get deformed to other shapes and produce less perfect or smaller recovery than the smaller droplets. Thus the melt elasticity of this blend is influenced by the dispersed SAN droplets. With increasing temperature the fluidity
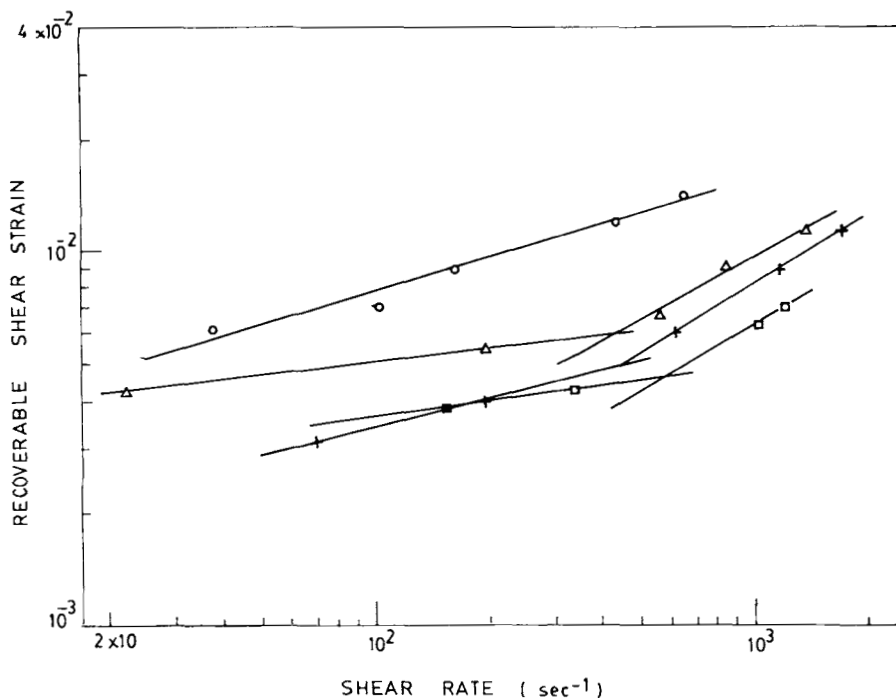
Figure 7 Recoverable shear strain as a function of shear rate at 210°C for PP–SAN blend at various compositions (wt % SAN): (O) 0; (△) 10; (+) 20; (□) 30.

increases, hence the recoverability of the droplets is reduced, which is in agreement with the observed decrease of melt elasticity of the blend with increas-

ing temperature. Furthermore, the observed decrease of blend composition dependence of S_R with increasing temperature is explainable by the decreased
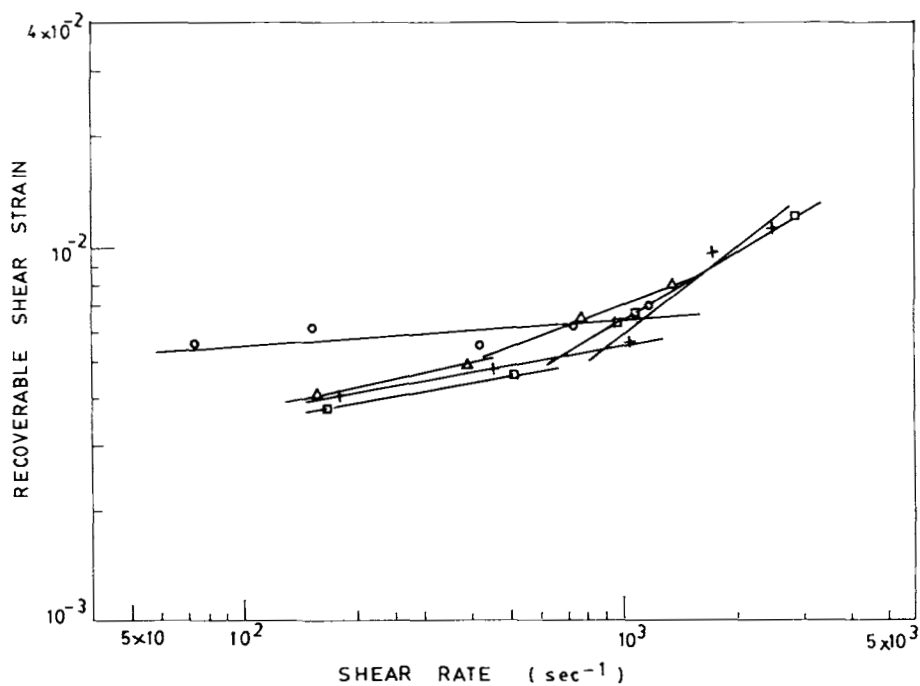
Figure 8 Recoverable shear strain as a function of shear rate at 230°C for PP-SAN blend at various compositions (wt % SAN): (O) 0; (△) 10; (+) 20; (□) 30.
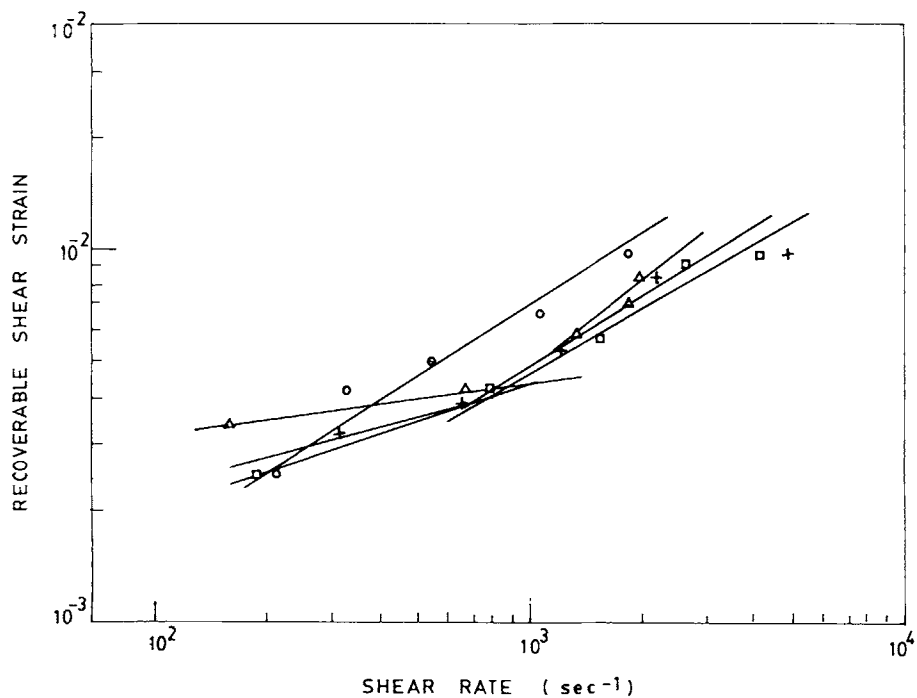
Figure 9 Recoverable shear strain as a function of shear rate at 250°C for PP-SAN blend at various compositions (wt % SAN): (O) 0; (△) 10; (+) 20; (□) 30.
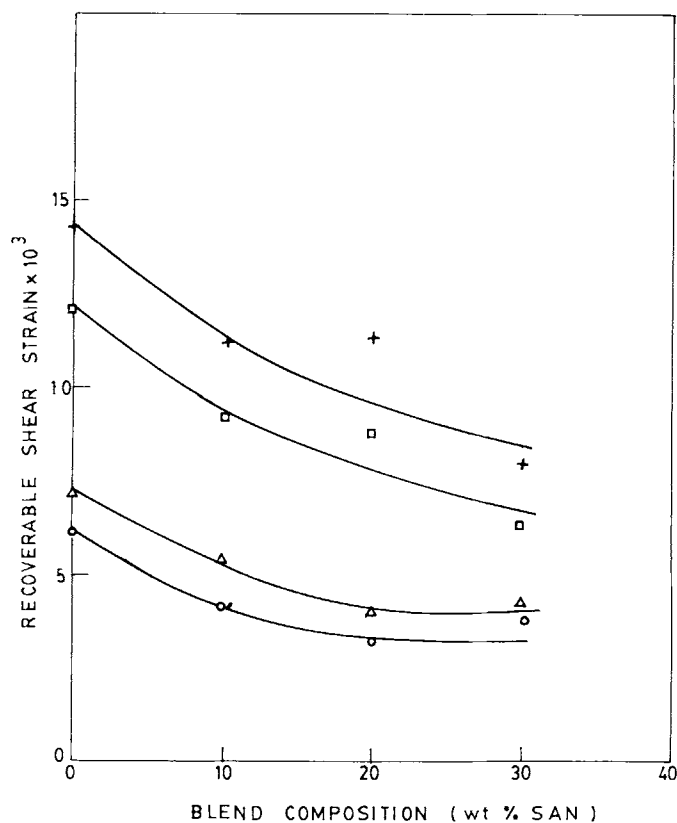
Figure 10 Recoverable shear strain as a function of blend composition for PP-SAN blend at 210°C at various shear stresses ($\times 10^5$ dyn/cm^2): (O) 3.67; (△) 6.12; (□) 11.2; (+) 13.5.
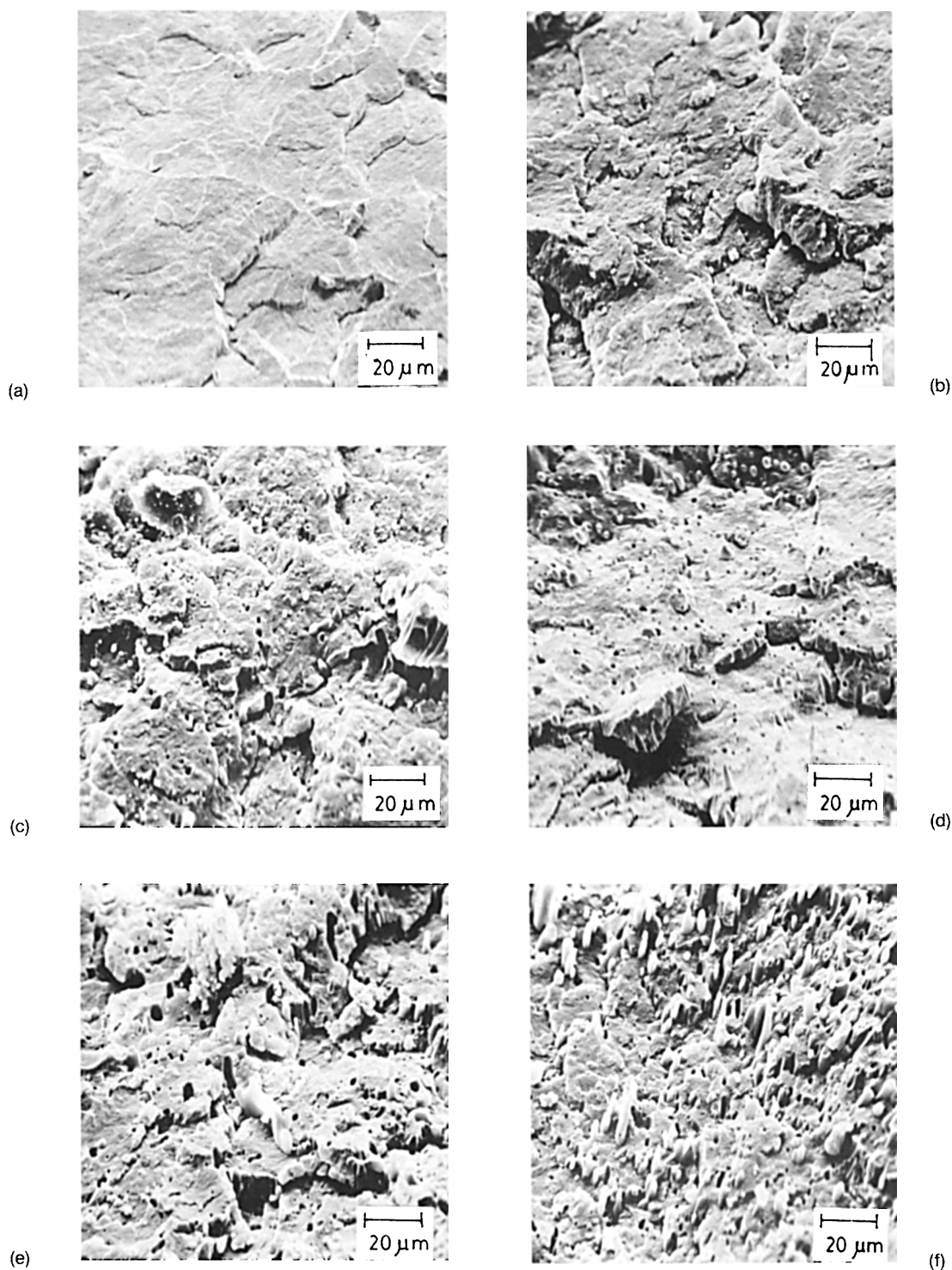
Figure 11 Scanning electron micrographs of cryogenically fractured surfaces of PP–SAN blend at various blend compositions (wt % SAN): (a) 0; (b) 5; (c) 10; (d) 15; (e) 20; (f) 30.

recoverability of droplets due to increased fluidity at higher temperatures.

Change of slope of S_R versus $\dot{\gamma}$ plot is a unique feature of this blend. Considering the significant role of the SAN component in the melt elasticity of the blend, the observed higher slope at the high shear rates suggest higher elastic recoverability of the droplets at shear rates greater than about 10^3 s^{-1}.

It appears that this limiting/critical shear rate corresponds to the formation of elongated droplets, which show more perfect elastic recovery than the spherical or irregular shaped droplets.

Melt elasticity as a function of composition decreases, as shown in Figure 10. This is accompanied by a decrease of melt viscosity (Fig. 5) of this blend with increasing SAN content. Though an increase of melt elasticity is generally accompanied by a decrease of melt viscosity, the present blend deviates from this general trend. This is presumably due to the unique role of the SAN droplets, which are sufficiently deformable and have good elastic recoverability to produce both ease of flow and increase in melt elasticity.

State of Dispersion

Scanning electron micrographs of the cryogenically fractured surfaces of the PP–SAN blend at different compositions are shown in Figure 11. The dispersion of SAN phase in PP matrix is quite good with fine and uniformly sized droplets of SAN dispersed homogeneously throughout. The droplets are so fine that at the smallest SAN content (5 wt %) they are visible only on a more careful look of the micrograph in comparison with the micrograph of unblended PP. As we proceed to higher SAN content, the droplets become more clearly distinguishable as small voids left over by the uprooted SAN component or as some elongated droplets of SAN projecting out from the surface. This elongation tendency of the SAN droplets is more prominantly apparent at higher SAN content (20 wt % and above), where the droplets are bigger and more in number.

Thus, uniform dispersion of SAN droplets in PP matrix, increase of droplet size with increasing SAN content, and the tendency of the droplets to form elongated shapes are the main features of this PP–SAN blend, which have been shown in the preceding section to explain the observed melt rheological behavior of this blend.

CONCLUSION

SAN copolymer forms a two-phase blend with PP with good dispersion of the SAN droplets in the PP matrix. The droplets show remarkable tendency of elongation, and the droplet size increases with increasing SAN content of the blend.

The melt of PP–SAN blend is non-Newtonian pseudoplastic at temperatures below 250°C, with a little variation of pseudoplasticity with SAN content.

The SAN droplets cause an ease of flow due to their tendency to elongate and align in flow direction. The reduction in melt viscosity is accompanied by a lowering of activation energy for viscous flow.

Melt elasticity of the blend also decreases with increasing SAN content, and its variation with shear rate shows two distinct slopes, suggesting a critical shear rate above which the SAN droplets acquire shapes suitable for good elastic recoverability.

REFERENCES

1. A. K. Gupta and S. N. Purwar, *J. Appl. Polym. Sci.,* **29,** 1079 (1984).
2. A. K. Gupta and S. N. Purwar, *J. Appl. Polym. Sci.,* **29,** 1595 (1984).
3. A. K. Gupta and S. N. Purwar, *J. Appl. Polym. Sci.,* **29,** 3513 (1984).
4. A. K. Gupta and S. N. Purwar, *J. Appl. Polym. Sci.,* **30,** 1777 (1985).
5. A. K. Gupta and S. N. Purwar, *J. Appl. Polym. Sci.,* **30,** 1799 (1985).
6. A. K. Gupta and S. N. Purwar, *J. Appl. Polym. Sci.,* **31,** 535 (1986).
7. L. A. Utracki and M. R. Kamal, *Polym. Eng. Sci.,* **22,** 96 (1982).
8. E. Martuscelli, C. Silvestre, and L. Bianchi, *Polymer,* **24,** 1458 (1983).
9. W. Ho and R. Salovey, *Polym. Eng. Sci.,* **21,** 839 (1981).
10. J. Ito, K. Mitani, and Y. Mizutani, *J. Appl. Polym. Sci.,* **29,** 75 (1984).
11. A. Rudin, D. A. Loucks, and J. M. Goldwasser, *Polym. Eng. Sci.,* **20,** 741 (1980).
12. A. Rudin and N. E. Brathwaite, *Polym. Eng. Sci.,* **24,** 1312 (1984).
13. C. D. Han, C. A. Villamizar, Y. W. Kim, and S. J. Chen, *J. Appl. Polym. Sci.,* **21,** 353 (1977).
14. A. K. Gupta, A. K. Jain, and S. N. Maiti, *J. Appl. Polym. Sci.,* **38,** 1699 (1989).
15. A. K. Gupta, A. K. Jain, B. K. Ratnam, and S. N. Maiti, *J. Appl. Polym. Sci.,* **39,** 515 (1990).
16. A. K. Gupta and B. K. Ratnam, *J. Appl. Polym. Sci.,* **42,** 297 (1991).
17. J. A. Brydson, *Plastics Materials,* Newnes-Butterworths, London, 1975.
18. C. B. Bucknall, *Toughend Plastics,* Applied Science, London, 1977.
19. C. D. Han, *Rheology in Polymer Processing,* Academic, New York, 1976, Chap. 5.
20. J. L. White, *J. Appl. Polym. Sci.,* **8,** 2339 (1964).
21. N. Tokita and J. L. White, *J. Appl. Polym. Sci.,* **10,** 1011 (1966).
22. J. L. White and N. Tokita, *J. Appl. Polym. Sci.,* **11,** 321 (1967).
23. R. I. Tanner, *J. Polym. Sci., A-2,* **8,** 2067 (1970).